NJC

ROYAL SOCIETY OF CHEMISTRY

PAPER

View Article Online
View Journal | View Issue

Cite this: *New J. Chem.*, 2020, **44**, 20751

An antibacterial composite film based on cellulose acetate/TiO_2 nanoparticles

Ying Gao, Xiu Wang, Xiang Li and Hongqi Dai *

Received 31st August 2020,
Accepted 15th October 2020

DOI: 10.1039/d0nj04374e

rsc.li/njc

In this study, cellulose acetate (CA)/titanium dioxide (TiO_2) composite films with different loadings (4 wt%–12 wt%) were prepared by the combination of ultrasonic dispersion, stirring and hot-pressing processes. Some properties of the films were characterized by techniques including SEM, XRD, FTIR spectroscopy, WCA analysis, tensile strength measurement, TGA, DSC and antibacterial analysis. The morphology and Ti element analysis mapping of the composite films were investigated through the methods of SEM. The results showed that the TiO_2 nanoparticles were successfully and uniformly connected with cellulose acetate. With the increase of TiO_2 content, the hydrophilic property of the films was enhanced. Films with different contents also maintained thermal stability and mechanical properties. The CA/TiO_2 film with 12 wt% loading exhibited good antibacterial activity against *Escherichia coli* with 55.6% sterilization in 12 h. Therefore, the CA/TiO_2 composite films can be applied as antibacterial films prepared by a simple method.

Introduction

Cellulose acetate (CA) is a biodegradable polymer formed from the acetylation of acetone,[1] with characteristics such as good toughness, high biocompatibility, good desalting, high potential flux, and relatively low cost.[2–4] Pure CA film, with high permeability, good filtration performance, excellent biocompatibility and blood compatibility properties, has been widely utilized in desalination, hemodialysis, and oil–water separation applications.[5] However, these applications always use CA films in water bodies with abundant microorganisms, meaning the films can be easily eroded and degraded by microorganisms in these complex water bodies.[6] As a linear polymer, CA is composed by betadehydrated glucose units and linked by C–O–C bonds, which makes CA films easy to degrade and erode by microbes.[7] This will not only shorten the service life of films, but also destroy their essential properties due to the destruction of the main structure. Therefore, providing CA films with antibacterial properties can widen their application.

The addition of nanoparticles such as zinc oxide,[8] titanium dioxide,[9] silver nanoparticles,[10] and copper nanoparticles[11] into films is widely used in antibacterial materials. TiO_2 as a typical nontoxic,[12] low cost, and efficient photocatalyst[13] has also been widely used in many other fields, such as electrochemistry,[14] hydrogen sensing,[15,16] detoxification processes,[17] and so on. The bactericidal and fungicidal effects of TiO_2 can work on a variety of microbes, including *Escherichia coli, Staphylococcus aureus, Pseudomonas aeruginosa* and *Penicillium expansum*.[18–23] The antimicrobial activity of TiO_2 is achieved due to the production of reactive oxygen species (ROS) such as hydroxyl radicals ($^{\bullet}OH$) and superoxide radical ($O_2^{-\bullet}$) upon illumination of UV-A light with a wavelength of 385 nm or lower.[24]

TiO_2 has been widely used in antibacterial composite films. Sima Asadi *et al.* prepared an antimicrobial and antioxidant film based on polylactic acid (PLA) modified with titanium dioxide and lycopene pigment with suitable color properties for active and intelligent packaging of food. The addition of TiO_2 nanoparticles enabled antimicrobial activity of the film against *Escherichia coli* and *Staphylococcus aureus*.[9] Samaneh Ghasemi *et al.* combined bacterial cellulose/polypyrrole/TiO_2-Ag as a biosensor to detect and measure the growth of 5 pathogenic bacteria.[25] Jing Xie *et al.* compared different biodegradable polymers (cellulose acetate (CA), polycaprolactone (PCL) and polylactic acid (PLA)) for food packaging films composited with TiO_2 nanoparticles, and the TiO_2 embedded CA film had the potential to be used as antimicrobial food packaging.[26] There are also many previous works that have combined cellulose acetate and TiO_2, in order to obtain composite materials with interesting properties that are suitable for different applications. Xiujuan Jin *et al.* designed a flexible mesoporous TiO_2 microspheres/cellulose acetate hybrid film as a high performance recyclable photocatalyst. The film was prepared by dispersing mesoporous TiO_2 microspheres onto the surface of a free-standing cellulose acetate film at room temperature, and it can be easily applied in the field of wastewater treatment without leaving any photocatalyst in the reaction system.[27] Reza Abedini *et al.* dispersed TiO_2 nanoparticles in CA casting solutions *via*

Jiangsu Co-Innovation Center of Efficient Processing and Utilization of Forest Resources, Nanjing Forestry University, Nanjing, 210037, China. E-mail: hgdhq@njfu.edu.cn

phase inversion to get CA/TiO_2 hybrid membranes. The addition of TiO_2 nanoparticles caused the hybrid membrane to become more porous, improve thermal stability and leading to an increase of water permeation.[28] However, the fabrication methods were complex (including ultrasonic dispersion, casting, irradiation, hybridization *etc.*), and the addition of some extra chemicals (methyl acetate, Ag nanoparticles, NPs *etc.*) was required to enhance the antibacterial ability or physical properties of the composites.

Because of their high specific surface area and surface energy, TiO_2 nanoparticles could easily aggregate and further limit antibacterial ability,[23,29] which makes it difficult to realize a homogeneous dispersion of TiO_2 in liquids. In this work, a homogeneous CA/TiO_2 composite film was fabricated through a combination of three steps, ultrasonic dispersion, vigorous stirring and hot pressing, which formed an easy to control preparation method without adding extra chemicals. The structure and properties of the composite films were characterized by using SEM, XRD, FTIR spectroscopy, water contact angle analysis, tensile strength measurement, TGA and DSC. The objectives of this paper were (1) to prevent the aggregation of TiO_2 nanoparticles to obtain a uniform suspension; (2) to obtain homogeneous composite films through three simple steps; (3) to evaluate the antibacterial properties of the CA/TiO_2 composite films against *E. coli* in water.

Materials and methods

Materials

Cellulose acetate (CA, 39.8 wt% acetyl group, 3.5 wt% hydroxyl group) was obtained from Shanghai Aladdin Biochemical Technology Co., Ltd (Shanghai, China). TiO_2 nanoparticles (99.8% purity, particle size: 40 nm) were obtained from Shanghai McLean Biochemical Technology Co., Ltd (Shanghai, China). Acetone, glycerol, ethanol and sodium chloride were obtained from Nanjing Chemical Reagent Co., Ltd (Nanjing, China). Yeast and soaking powder were obtained from Beijing Aobo Biotechnology Co., Ltd (Beijing, China). Peptone and purified agar powder were obtained from Shanghai Bowei Biotechnology Co., Ltd (Shanghai, China).

CA/TiO_2 composite film preparation

The preparation process of the CA/TiO_2 composite film is shown in Fig. 1. Taking CA–4 wt% TiO_2 as an example, 0.26 g of TiO_2 was added into 10 mL of acetone; a uniform suspension was obtained by using an ultrasonic cell breaker (XO-650, Nanjing Xianou Instrument Manufacturing Co., Ltd) at 650 W for 30 minutes. The casting solution was prepared by mixing 6.5 g of CA, 40 mL of acetone, 5 mL of glycerol and 10 mL of TiO_2 suspension in a 250 mL flask and stirring at 60 °C at 300 rpm for 1 h. After that, 3 g of the casting solution was poured into a Petri dish in a fume hood and cooled to forming. The Petri dish was placed into a dryer filled with ethanol to remove acetone with ethanol absorption effectively. Then, the film was taken out and immersed in deionized water (DIW) for 6 hours to remove residual acetone. The composite film was obtained after drying and hot-pressing (XW212C, Xunwei Testing Instrument Co., Ltd). The pressing time was 3 minutes at 100 °C and 2.5 MPa. Then, the dry film was kept in a sealed bag.

Characterization

The morphology of the CA/TiO_2 films was observed using scanning electron microscopy (SEM, Carl Zeiss NTS, Peabody, MA). The X-ray diffraction (XRD, Rigaku Corp., Tokyo, Japan) patterns of the composite films were recorded at 50 kV and 50 mA in the range of 2θ = 10°–80° at a scanning rate of 4° min^{-1} (aa). The FT-IR (Nicolet 6700, Thermo Scientific, USA) spectra were recorded in the range from 4000 to 0 cm^{-1} (Amiri) with scanning 32 times, and sample preparation used a potassium bromide tablet method. The dynamic water contact angle (WCA) of the films was determined by performing the sessile drop method using a contact angle analyzer (Attention Theta, Biolin Scienfic, Inc. Stockholm, Sweden). Each measurement was conducted for 10 s, and an average value was presented. The mechanical properties of the composite films were tested by an electronic universal testing machine (UTM8502, Shenzhen Sansi Longitudinal and Horizontal Technology Co., Ltd); the sample was pulled apart at a head speed of 2 mm min^{-1} with a loading of 100N. Each film was tested after being immersed in water for 30 minutes. Thermogravimetric analysis (TGA) of the films was employed using a Pyris 1 thermogravimetric analyzer (NETZSCH, TG 209F1, Germany). The mass of the samples was about 10 mg. The samples were heated from 50 to 500 °C with a heating rate of 10 °C min^{-1} under an inert atmosphere of nitrogen at a gas flow of 20 mL min^{-1}. Differential scanning calorimetry (DSC 214 Polyma Netzsch, German) of the films was performed with heating from

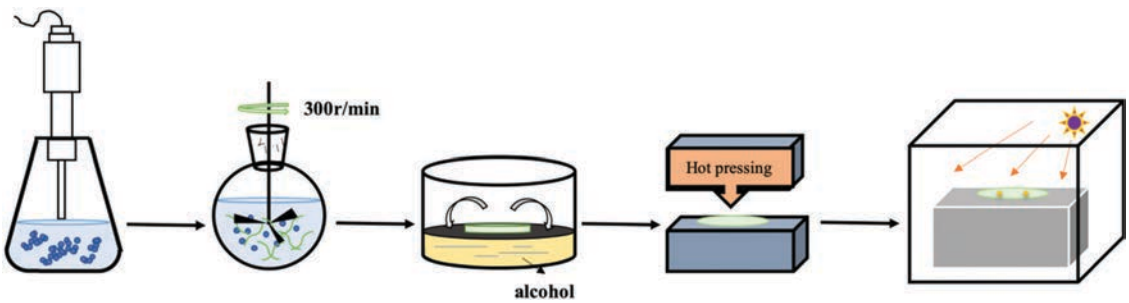

Fig. 1 Preparation process of the CA/TiO_2 composite film.

50 to 300 °C with a heating rate of 10 °C min^{-1} under an inert atmosphere of nitrogen at a gas flow of 40 mL min^{-1}.

Antibacterial activity of the composite films against *E. coli*

E. coli was used for measuring the antibacterial properties of the composite films. The composite films were cut into pieces and added into an *E. coli* suspension. After 24 hours, the colony experiment was carried out to count the number of colonies. 50 μL of *E. coli* seed liquid (cgmcc 1.8723) and 5 mL of liquid medium were added into a glass shaking tube. The mixture was evenly mixed and cultured at 37 °C and 200 rpm for 12 h in a constant temperature shaker. 0.2 mL of activated *E. coli* solution, 10 mL of saline, 0.5 mL of liquid medium, and 0.5 g of the shredded composite film were added into a centrifuge; meanwhile, the blank control was the sample without the composite film. All the centrifugal tubes were placed in a constant temperature incubator at 37 °C for 24 h under ultraviolet light for photocatalytic reaction. Then, 0.1 mL of the *E. coli* solution after 24 h growth of each sample was diluted 10^6 times. 0.2 mL of the diluted solution was coated evenly on agar medium. After the diluted solution was completely absorbed by nutrient agar, the Petri dishes were cultured in a constant temperature and humidity incubator at 37 °C. After 24 h, the number of colonies in the Petri dishes was counted and the inhibition ratio was calculated.

The formula for calculating inhibition ratio is shown as eqn (1):

$$AA = N_{sc} - N_s/N_{sc} \times 100\% \quad (1)$$

Here, N_{sc} is the control colony without composite films, N_s is the colony with the composite films with different TiO_2 loadings, and AA is the inhibition ratio. The higher the AA value, the stronger the antibacterial properties.

Results and discussions

Morphology of CA/TiO_2 composite film

The composite films were prepared by using CA and TiO_2 nanoparticles. The surface morphology of the composite films was studied using SEM, and the Ti element was mapped by EDS to verify the dispersion of TiO_2 nanoparticles clearly. The surface morphology of the CA-12 wt% TiO_2 composite film with ultrasonic dispersion is shown in Fig. 2a and b. As shown in Fig. 2a, all the TiO_2 nanoparticles are homogeneously distributed on the CA fiber surface, and CA and TiO_2 nanoparticles are combined with each other tightly, indicating that ultrasonication could reduce the particle aggregation effectively. Fig. 2b shows the film with 12 wt% TiO_2 content after hot-pressing, which has a flat surface. By using this method, TiO_2 nanoparticles have been dispersed uniformly without aggregation on the film. Meanwhile, stirring could prevent re-aggregation of the TiO_2.

Fig. 2c shows the cross-section SEM image of the CA-12 wt% TiO_2 composite film. We can see that there was no obvious stratification phenomenon on the cross-section, indicating that the components in the casting solution were mixed evenly.

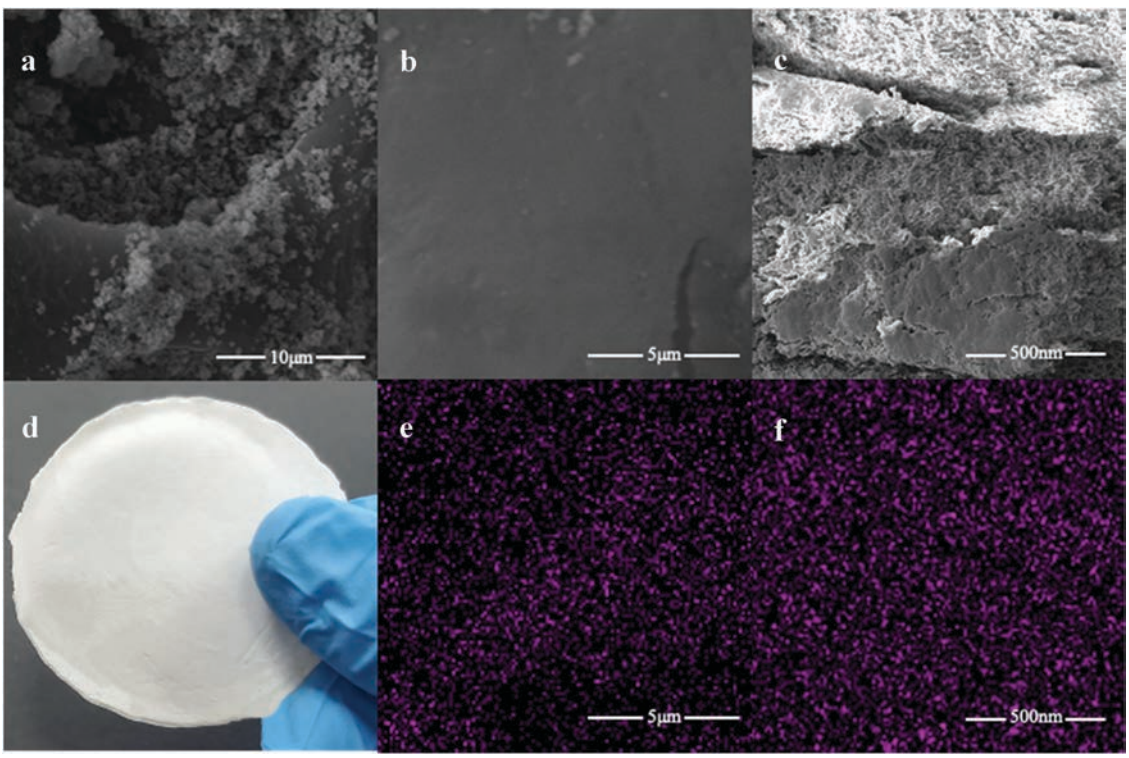

Fig. 2 (a) The surface SEM image of the CA-12 wt% TiO_2 film before hot-pressing; (b) the surface SEM image of the CA-12 wt% TiO_2 film; (c) the cross-section SEM image of the CA-12 wt% TiO_2 film; (d) digital image of the CA-12 wt% TiO_2 film. (e and f) The surface (figure b) and cross-section (figure c) EDS Ti element analysis maps of the CA-12 wt% TiO_2 film.

After sonication, stirring and hot-pressing, the film became relatively stable. The purple light spot in Fig. 2e and f represents the Ti element. As can be seen from the figures, the distribution of TiO_2 nanoparticles was uniform on both the surface (Fig. 2e) and cross-section (Fig. 2f), which further revealed that the ultrasonic dispersion and stirring could make the TiO_2 nanoparticles evenly dispersed in the casting solution.

FTIR and XRD analysis of CA/TiO_2 composite films

Fig. 3a shows the FT-IR spectra of the CA film and CA/TiO_2 composite film. All spectra show several absorption features from 500 cm^{-1} to 4000 cm^{-1}. These major absorption features appeared at 1732 cm^{-1} (–C═O), 1451 cm^{-1} (O═C–OR), 1369 cm^{-1} ($–CH_2$), 1217 cm^{-1} (C–O), 1032 cm^{-1} (C–O–C) and 900 cm^{-1} (–CH). The features above 2000 cm^{-1} are both intense and composition sensitive. The signals appeared at 2922 cm^{-1} ($–CH_2$) and 3700–3200 cm^{-1} (–OH) as characteristic bands of CA, especially in the presence of both –OH and the characteristic stretching bands at 3700–3200 cm^{-1}.[30] All the samples exhibited similar characteristic features without introducing any new peaks. The results demonstrated that only physical blending and no chemical reaction occurred between the TiO_2 nanoparticles and CA.

Fig. 3b shows the XRD patterns of the CA film and CA/TiO_2 composite film. It can be observed that the pattern of TiO_2 nanoparticles has three characteristic crystalline peaks at 2θ values of 24.37, 38.431, and 48.614 corresponding to anatase, rutile and brookite, respectively.[9] According to the X-ray diffraction patterns of CA/TiO_2-4 wt%, CA/TiO_2-8 wt%, and CA/TiO_2-12 wt%, new peaks were generated, which confirmed the crystal structure of titanium dioxide nanoparticles. TiO_2 will also partially crystallize the CA film.

Hydrophilicity of the CA/TiO_2 composite film

Fig. 4 shows the water contact angle (WCA) of the CA/TiO_2 composite films with different loadings of TiO_2 nanoparticles. The primary WCA of the composite films was 65.63°, 58.03°, 56.51° and 54.07° for TiO_2 loadings increasing from 0 to 12 wt%, respectively. TiO_2 nanoparticles could enhance the hydrophilicity of the composite film obviously. Under the irradiation of ultraviolet (UV) light, TiO_2 nanoparticles excite their electron hole pairs, which react with Ti^{4+} and O^{2-} on their surface, generating Ti^{3+} and oxygen vacancies. Oxygen vacancies can easily adsorb water from the air, forming a hydrophilic micro area around them, thus improving the hydrophilicity of the composite film.[31,32] After 10 s, the average WCA was decreased to 62.55°, 54.23°, 52.6° and 50.65° for TiO_2 nanoparticle loadings increasing from 0 to 12 wt%, respectively. With the increase of the retention time of the droplets on the films, the WCAs of the composite films all decreased by about 4° with respect to the initial WCAs because of the hydrophilic micro-area formation. Therefore, the addition of TiO_2 nanoparticles improved the hydrophilic performance, which made the films more suitable for use in a water environment.

Wet mechanical properties of the CA/TiO_2 composite film

CA film is mostly used in aqueous medium accompanied by a certain pressure,[5] and the application potential can be

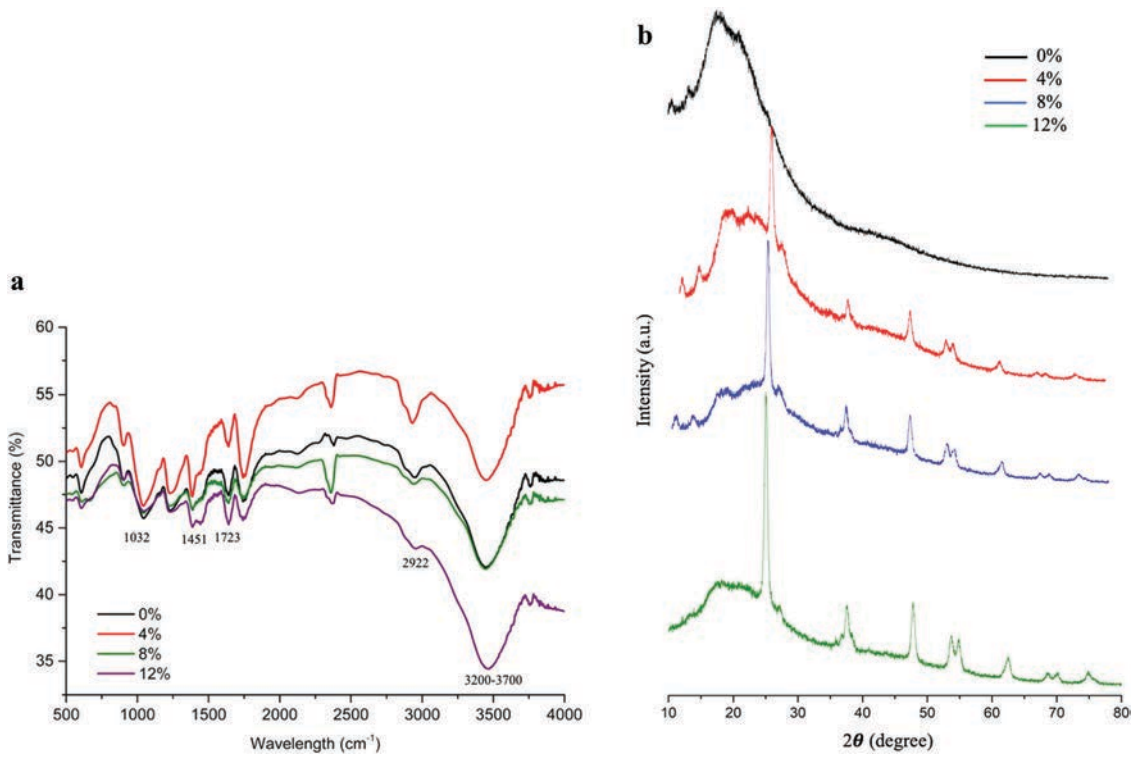

Fig. 3 (a) FT-IR spectra of CA/TiO_2 composite films with different TiO_2 contents; (b) X-ray diffraction patterns of CA/TiO_2 composite films with different TiO_2 contents.

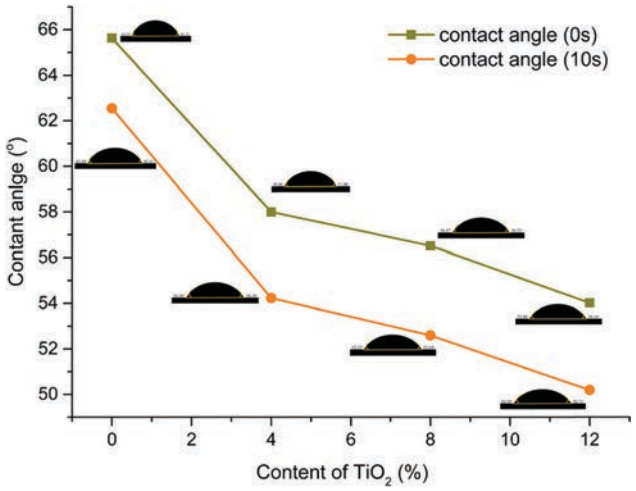

Fig. 4 Water contact angle (WCA) of the composite films with different TiO_2 loadings.

influenced by the wet mechanical properties. Here, the tensile strength, elongation at break and young's modulus of the composite films were tested systematically after the composite films were immersed in water for 30 min.

As shown in Table 1, the wet tensile strength and elongation at break of the composite films first increased and then decreased with the increase of TiO_2 loading. The tensile strengths of the pure CA film and CA-4 wt% TiO_2 film were 4.29 MPa and 7.15 MPa, respectively. However, the tensile strength showed a decreasing trend from 7.15 MPa to 5.69 MPa when the TiO_2 loading increased from 4 wt% to 12 wt%. Meanwhile, the elongation at break showed the same tendency. The CA-4 wt% TiO_2 film showed the highest elongation at break of 6.25%, but the highest Young's modulus value appeared at 8 wt% TiO_2 content as 424.79 MPa. This suggested that a small amount of TiO_2 nanoparticles could disperse uniformly inside the composite films, and some of the TiO_2 could connect with the CA by hydrogen bonding, which improved the mechanical properties of the composite films effectively. When the TiO_2 loading increased further, the hydrogen bonds between CA fibers were blocked, and the bonding strength between fibers was gradually reduced, resulting in the tensile strength decrease of the composite film. Meanwhile, when the film had a higher TiO_2 loading, the TiO_2 nanoparticles underwent aggregation and produced a stress concentration phenomenon, which also led to the decline of wet tensile strength of the film. Furthermore, with increasing TiO_2 content, more Ti–OH_2 groups were formed on the TiO_2 nanoparticle surface and they strengthened the hydrogen bonding. The hydrogen bonding made it difficult to achieve relative sliding inside the composite film,[33] thus the elongation at break decreased continuously. A similar result was observed in the Young's modulus test, which was also attributed to the aggregation of TiO_2 nanoparticles at a higher loading. However, adding TiO_2 to the composite films led to stronger mechanical properties, which further confirmed the strong interactions between TiO_2 nanoparticles and CA.

Table 1 Physical properties of CA/TiO_2 composite films with different TiO_2 contents

Films abbreviation	Tensile strength (MPa)	Elongation at break (%)	Young's modulus (MPa)
Pure CA	4.29	2.96	234.26
CA-4 wt% TiO_2	7.15	6.25	280.96
CA-8 wt% TiO_2	5.79	4.74	424.79
CA-12 wt% TiO_2	5.69	2.40	239.51

Thermal stability of the CA/TiO_2 composite film

Fig. 5a shows the weight loss (TG) curve of the composite membrane in a N_2 atmosphere. The thermal transition of the films occurred in the range of 200–500 °C. Before the temperature reached 300 °C, the mass loss of all composite films was only about 10%, and films lost most weight between 300 °C and 350 °C. At around 300 °C, the composite films softened and burnt, and the color also changed at 350 °C. With increasing temperature, intermolecular hydrogen bonding weakened and thermal stability decreased. The thermal transition included three phases: (1) intermolecular and intramolecular hydrogen bonds were affected by temperature and thermal movement; (2) the thermal decomposition of organic matter (intermolecular and intramolecular dehydration); (3) decomposition of residues. Fig. 5 shows that the thermal stability of the composite films did not change with the TiO_2 content. This is because TiO_2 has good thermal stability and there was a strong hydrogen bond between CA and TiO_2 nanoparticles.[33] On the other hand, this could be attributed to the catalytic properties of TiO_2 nanoparticles, which facilitated a faster breakdown of the cross-linking in the carbon skeleton.

Fig. 5b shows the DSC results in the temperature range of 50–300 °C of different composite films. For the pure CA film, the glass transition (T_g) and melting (T_m) temperatures of CA are known to be around 198–205 °C and 224–230 °C, respectively.[30] All the composite films were hot-pressed at 100 °C, so the result indicates the absence of a dehydration endotherm. There are some endotherms observed between 185 and 225 °C. The last endotherm at 225 °C shows the melting temperature (T_m) of the composite film, which is in accordance with the literature.[30] The endotherms before 225 °C were due to the gradual removal of the acetyl groups of CA. Otherwise, there is no difference between the different films, confirming the strong interactions between TiO_2 nanoparticles and CA.

Antibacterial activity of the CA/TiO_2 composite film

The antibacterial activity of the composite films against *E. coli* is shown in Table 2. There was an obvious difference in antibacterial activity among the different films. After adding the composite films into the bacterial solution, the number of *E. coli* colonies in the culture dish was significantly reduced, which showed a certain antibacterial activity of the CA/TiO_2 composite films. The bactericidal rate of the composite films were 25.00%, 41.67% and 55.56%, respectively, indicating that TiO_2 had a significant antibacterial ability in reducing the growth of *E. coli*. With increasing TiO_2 loading, the number

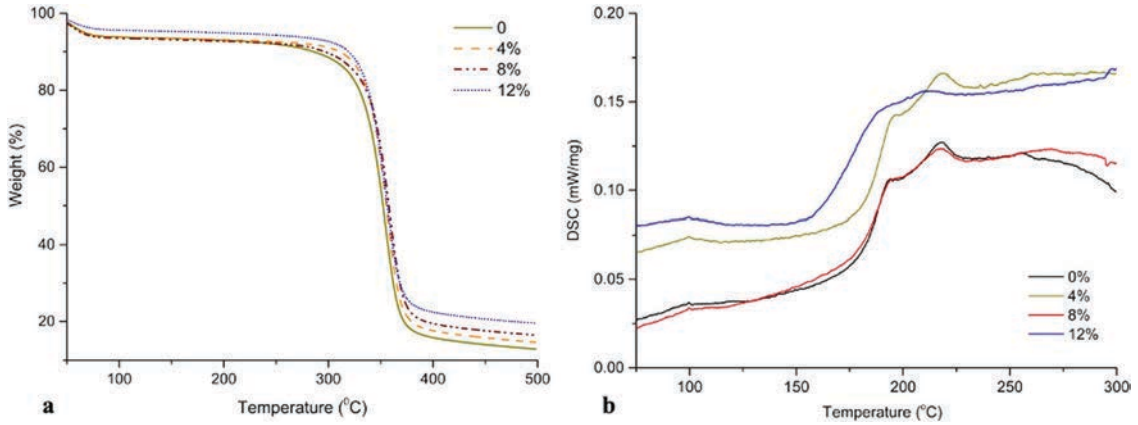

Fig. 5 (a) TGA curves of CA/TiO_2 composite films with different TiO_2 contents; (b) the DSC spectra of CA/TiO_2 composite films with different TiO_2 contents.

Table 2 Inhibition ratio of composite films with different TiO_2 contents

TiO_2 content (wt%)	0	4 wt%	8 wt%	12 wt%
Number of colony groups	36	27	21	16
Inhibition rate (%)	0	25.00	41.67	55.56

of *E. coli* colonies decreased. Due to the photocatalytic reaction of TiO_2 nanoparticles, the components on the *E. coli* cell surface and in the cell were destroyed. Under the condition of photocatalysis, the TiO_2 surface produced electron–hole pairs. Hydroxyl radicals ($^{\bullet}OH$) and reactive oxygen species (ROS) generated on the illuminated TiO_2 surface played a role in inactivating microorganisms by oxidizing the polyunsaturated phospholipid component of the *E. coli* cell membrane.[6,21,31,34–36] These active oxidants had high reactivity, and they could oxidize and degrade organic matter and destroy the structure of *E. coli* cell membrane and the living environment. Meanwhile, when the microorganism was attacked by TiO_2 photocatalysis, the *E. coli* cell wall was destroyed first, then the plasma membrane, which eventually led to the attack of intracellular substances.[37,38] Therefore, with the increase of TiO_2 content, more active ions such as hydroxyl radicals in the bacterial suspension enhanced the antibacterial properties.

Conclusions

The CA/TiO_2 composite film was fabricated by an easy method, *i.e.*, the combination of ultrasonic dispersion, stirring and hot-pressing. Through ultrasonic dispersion, the agglomerates of TiO_2 nanoparticles could be dispersed uniformly in acetone solvent and mixed with CA homogeneously. With the increase of TiO_2 content, the bactericidal rate of the composite film increased from 25.00% (4 wt% TiO_2 loading) to 55.56% (12 wt% TiO_2 loading). The analysis of physical properties revealed that the TiO_2 nanoparticles did not decrease the tensile strength and elongation at break of the composite films after immersion in water for 30 min. Meanwhile, the TiO_2 nanoparticles could form hydrogen bonds with CA because of the presence of –OH groups on the TiO_2 surface, which could improve the hydrophilic performance of the composite films effectively. The 12 wt% TiO_2 loaded film displayed hydrophilic properties with a WCA of 50.65°, a decrease of 11.9° compared to the non-TiO_2 one. Therefore, TiO_2 nanoparticles were combined with CA and became a homogenous composite film using a flexible method without adding other chemicals, which will have broad application potential in the water treatment field.

Author contribution

Ying Gao performed the experiments, analyzed the data, and wrote the manuscript. Xiu Wang performed part of the experiment and edited the manuscript. Xiang Li performed the XRD, FTIR and DSC measurement. Hongqi Dai conceived the idea and supervised the work.

Conflicts of interest

The authors declare no competing financial interest.

Acknowledgements

We acknowledge financial support from the National First-class Disciplines (PNFD) and a project funded by the Priority Academic Program Development of Jiangsu Higher Education Institutions (PAPD).

References

1 D. M. Gouvêa, R. C. S. Mendonça, M. L. Soto and R. S. Cruz, Acetate cellulose film with bacteriophages for potential antimicrobial use in food packaging, *LWT--Food Sci. Technol.*, 2015, **63**, 85–91.
2 A. Idris and L. K. Yet, The effect of different molecular weight PEG additives on cellulose acetate asymmetric dialysis membrane performance, *J. Membr. Sci.*, 2006, **280**, 920–927.

3 M. Hayama, K. I. Yamamoto, F. Kohori and K. Sakai, How polysulfone dialysis membranes containing polyvinylpyrrolidone achieve excellent biocompatibility?, *J. Membr. Sci.*, 2004, **234**, 41–49.
4 E. Ferjani, R. H. Lajimi, A. Deratani and M. S. Roudesli, Bulk and surface modification of cellulose diacetate based RO/NF membranes by polymethylhydrosiloxane preparation and characterization, *Desalination*, 2002, **146**, 325–330.
5 J. Puls, S. A. Wilson and D. Hölter, Degradation of Cellulose Acetate-Based Materials: A Review, *J. Polym. Environ.*, 2011, **19**, 152–165.
6 X. Yin, *et al.*, Comparison of succinylation methods for bacterial cellulose and adsorption capacities of bacterial cellulose derivatives for Cu^{2+} ion, *Polym. Bull.*, 2011, **67**, 401–412.
7 E. Feese, H. Sadeghifar, H. S. Gracz, D. S. Argyropoulos and R. A. Ghiladi, Photobactericidal porphyrin-cellulose nanocrystals: Synthesis, characterization, and antimicrobial properties, *Biomacromolecules*, 2011, **12**, 3528–3539.
8 M. Rezaei, S. Pirsa and S. Chavoshizadeh, Photocatalytic/Antimicrobial Active Film Based on Wheat Gluten/ZnO Nanoparticles, *J. Inorg. Organomet. Polym. Mater.*, 2020, **30**, 2654–2665.
9 S. Asadi and S. Pirsa, Production of Biodegradable Film Based on Polylactic Acid, Modified with Lycopene Pigment and TiO_2 and Studying Its Physicochemical Properties, *J. Polym. Environ.*, 2020, **28**, 433–444.
10 K. Yorseng, S. Siengchin, B. Ashok and A. V. Rajulu, Nanocomposite egg shell powder with in situ generated silver nanoparticles using inherent collagen as reducing agent, *J. Bioresour. Bioprod.*, 2020, **5**, 101–107.
11 B. Ashok, N. Hariram, S. Siengchin and A. V. Rajulu, Modification of tamarind fruit shell powder with in situ generated copper nanoparticles by single step hydrothermal method, *J. Bioresour. Bioprod.*, 2020, **5**, 180–185.
12 J. Zhang, Q. Xu, Z. Feng, M. Li and C. Li, Importance of the Relationship between Surface Phases and Photocatalytic Activity of TiO2, *Angew. Chem., Int. Ed.*, 2008, **120**, 1790–1793.
13 Z. He, *et al.*, A visible light-driven titanium dioxide photocatalyst codoped with lanthanum and iodine: An application in the degradation of oxalic acid, *J. Phys. Chem. C*, 2008, **112**, 16431–16437.
14 M. Tian, G. Wu, B. Adams, J. Wen and A. Chen, Kinetics of photoelectrocatalytic degradation of nitrophenols on nanostructured TiO_2 electrodes, *J. Phys. Chem. C*, 2008, **112**, 825–831.
15 O. K. Varghese, *et al.*, Extreme Changes in the Electrical Resistance of Titania Nanotubes with Hydrogen Exposure, *Adv. Mater.*, 2003, **15**, 624–627.
16 O. K. Varghese, D. Gong, M. Paulose, K. G. Ong and C. A. Grimes, Hydrogen sensing using titania nanotubes, *Sens. Actuators, B*, 2003, **93**, 338–344.
17 Z. Zhang, *et al.*, Photoelectrocatalytic activity of highly ordered TiO2 nanotube arrays electrode for azo dye degradation, *Environ. Sci. Technol.*, 2007, **41**, 6259–6263.
18 Y. S. Choi and B. W. Kim, Photocatalytic disinfection of E coli in a UV/TiO_2-immobilised optical-fibre reactor, *J. Chem. Technol. Biotechnol.*, 2000, **75**, 1145–1150.
19 J. Wist, J. Sanabria, C. Dierolf, W. Torres and C. Pulgarin, Evaluation of photocatalytic disinfection of crude water for drinking-water production, *J. Photochem. Photobiol., A*, 2002, **147**, 241–246.
20 B. Kim, D. Kim, D. Cho and S. Cho, Bactericidal effect of TiO_2 photocatalyst on selected food-borne pathogenic bacteria, *Chemosphere*, 2003, **52**, 277–281.
21 P. C. Maness, *et al.*, Bactericidal activity of photocatalytic TiO_2 reaction: Toward an understanding of its killing mechanism, *Appl. Environ. Microbiol.*, 1999, **65**, 4094–4098.
22 C. Maneerat and Y. Hayata, Antifungal activity of TiO_2 photocatalysis against Penicillium expansum in vitro and in fruit tests, *Int. J. Food Microbiol.*, 2006, **107**, 99–103.
23 A. Yousefi, A. Allahverdi and P. Hejazi, Effective dispersion of nano-TiO_2 powder for enhancement of photocatalytic properties in cement mixes, *Constr. Build. Mater.*, 2013, **41**, 224–230.
24 A. O. Ibhadon and P. Fitzpatrick, Heterogeneous photocatalysis: Recent advances and applications, *Catalysts*, 2013, **3**, 189–218.
25 S. Ghasemi, M. R. Bari, S. Pirsa and S. Amiri, Use of bacterial cellulose film modified by polypyrrole/TiO2-Ag nanocomposite for detecting and measuring the growth of pathogenic bacteria, *Carbohydr. Polym.*, 2020, **232**, 115801.
26 J. Xie and Y. C. Hung, UV-A activated TiO_2 embedded biodegradable polymer film for antimicrobial food packaging application, *LWT*, 2018, **96**, 307–314.
27 X. Jin, *et al.*, Flexible TiO_2/cellulose acetate hybrid film as a recyclable photocatalyst, *RSC Adv.*, 2014, **4**, 12640–12648.
28 R. Abedini, S. M. Mousavi and R. Aminzadeh, A novel cellulose acetate (CA) membrane using TiO2 nanoparticles: Preparation, characterization and permeation study, *Desalination*, 2011, **277**, 40–45.
29 X. Zhang, *et al.*, Preparation of chitosan-TiO_2 composite film with efficient antimicrobial activities under visible light for food packaging applications, *Carbohydr. Polym.*, 2017, **169**, 101–107.
30 E. A. Al Matroushi, Y. E. Greish, M. A. Meetani and B. A. Al Shamisi, Application of cellulose acetate fibrous membranes in the removal of micro- and submicron solid particulates in drinking water media, *Desalin. Water Treat.*, 2016, **57**, 15676–15686.
31 S. Sébastien, Les soignants face à la mort, *Rev. Infirm*, 2012, **1**, 39–41.
32 A. L. Linsebigler, G. Lu and J. T. Yates, Photocatalysis on TiO2 Surfaces: Principles, Mechanisms, and Selected Results, *Chem. Rev.*, 1995, **95**, 735–758.
33 J. Wang, *et al.*, Preparation of cellulose fiber-TiO_2 nanobelt-silver nanoparticle hierarchically structured hybrid paper and its photocatalytic and antibacterial properties, *Chem. Eng. J.*, 2013, **228**, 272–280.
34 T. Saito, T. Iwase, J. Horie and T. Morioka, Mode of photocatalytic bactericidal action of powdered semiconductor TiO_2 on mutans streptococci, *J. Photochem. Photobiol., B*, 1992, **14**, 369–379.

35 Z. Huang, *et al.*, Bactericidal mode of titanium dioxide photocatalysis, *J. Photochem. Photobiol., A*, 2000, **130**, 163–170.
36 K. P. Kühn, *et al.*, Disinfection of surfaces by photocatalytic oxidation with titanium dioxide and UVA light, *Chemosphere*, 2003, **53**, 71–77.
37 H. M. Yadav, J. S. Kim and S. H. Pawar, Developments in photocatalytic antibacterial activity of nano TiO_2: A review. *Korean*, *J. Chem. Eng.*, 2016, **33**, 1989–1998.
38 T. Ohno, T. Mitsui and M. Matsumura, Photocatalytic activity of S-doped TiO_2 photocatalyst under visible light, *Chem. Lett.*, 2003, **32**, 364–365.

